

NUMERICAL INVESTIGATION OF THE WAKE AFFECTED UNSTEADINESS ON FLAT PLATE BOUNDARY LAYER

Sanchita Amin* and Dipak Kanti Das

Department of Mechanical Engineering,
Bangladesh University of Engineering and Technology, Dhaka-1000

*Corresponding e-mail: sanchita@me.buet.ac.bd

Abstract: The present numerical simulation has been conducted with the aim to observe the unsteady boundary layer characteristics on a flat plate induced by a von Karman vortex street wake. This flow situation is an idealization of that occurring on turbomachinery blades where unsteady wakes are generated by the preceding row of blades. In this research, the boundary layer is developed under zero pressure gradients while the vortex street is generated by an elliptic cylinder positioned in the free stream. The minor-major axes ratio of the elliptic cylinder is taken as 0.6 with an angle of attack 0° . The investigation has been performed for different cylinder-to-plate relative position and a Reynolds number of 500 based on the focal distance of the elliptic cylinder and free stream velocity. The time dependent, two dimensional flow is simulated numerically. The consequent mathematical model is governed by the coupled equations of mass, and momentum and solved by employing Galerkin weighted residual method of finite element formulation. The development of the flow field up to certain time period is considered. Instantaneous streamlines of the disturbed flow field, instantaneous velocity field, boundary layer integral parameters, and skin friction on different streamwise locations on the plate are presented in this paper. The result shows that the wake vortices strongly affect the boundary layer over the flat plate.

Keywords: Wake, Boundary Layer, Separation Bubble, Skin Friction

INTRODUCTION

There are situations in aeronautics and turbo machinery where boundary layer transition originates from boundary layer interaction with transverse or longitudinal vortices. Upstream and downstream blade interactions in the passages of multi-stage axial turbo machines result in a complex and inherently unsteady flow field. In turbines and compressors, the relative motion of adjacent blade rows and consequently the wakes exhibit a defect in mean velocity and a superimposed high level of turbulence intensity. These conditions have a significant influence upon boundary layer transition process. the transition region of boundary layer affects the machine performance, the flow losses and especially the heat transfer to turbine blades. Hence, good understanding of the unsteady boundary layer behavior is important for improving the design of turbomachines.

Engineering applications often involve flows over complex bodies like wings, submarines, missiles, and rotor blades, which depends on parameters such as thickness ratio and angle-of-attack and these parameters greatly influence the nature of separation and the wake structure. Elliptic cylinders, which are more general geometrical configurations than the canonical circular cylinder, can provide a richer flow behavior characteristic of typical engineering flow configurations and significantly augment the understanding of wake flows.

Badr et al. (2001) solved numerically the problem of uniform flow past an impulsively started inclined elliptic cylinder for Reynolds numbers ranging from 900 to 5000 and for the range of angle of attack between 0 and 90° . The results reveal an unusual phenomenon of negative lift occurring shortly after the start of motion depending upon the value of the angle of inclination and are consistent with the experimental findings of Taneda (1972, 1977). A study was made on the process of laminar to turbulent transition induced by the von Karman vortex street, in the boundary layer on a flat plate by Kyriakides et al. (1996). It was established that, the onset of the strong von karman wake induced transition process was a function of the free stream velocity, the position of the cylinder with respect to the plate, the cylinder diameter, the drag coefficient and the minimum velocity in the developing wake at the streamwise position of the onset of the boundary layer transition. It was also established that, in the case of weak wake-boundary layer interaction, the boundary layer transition process was accelerated by the overall free stream turbulence increase due to the wake of the cylinder. Liu and Rodi (1991) investigated in detail the development of boundary layer along a flat plate under the influence of periodically passing wakes by hot-wire measurements. When wakes passed over the plate, the boundary layer was found to be turbulent quite early underneath the free-stream disturbances due to wakes, while it remained initially laminar. Victor O.

et al. (2006) carried out direct and large-eddy simulations of the interaction between a laminar boundary layer and a von Karman vortex street behind a circular cylinder for three values of the Reynolds number based on the cylinder diameter and free-stream velocity: $Re_D = 385, 1155$ and 3900 . Rapid, bypass-like transition to turbulence was observed in the two higher-Reynolds-number cases. Choi and Lee (2000) experimentally investigated the flow characteristics around an elliptic cylinder with an axis ratio (AR) of 2 located near a flat plate. In the near-wake region, the vortices were shed regularly only when the gap ratio was greater than the critical value of $G/B=0.4$, where G is the vertical distance between the plate and the cylinder and B is the length of minor axis of the cylinder. As the gap ratio increased, the drag co-efficient of the cylinder itself increased, but lift co-efficient decreased.

In the current research, numerical simulations have been performed to study the interaction between the unsteady wake of an upstream element and the boundary layer over a downstream element. To study such flows in a simpler setting, a model problem is considered, illustrated in Fig. 1, which consists of an elliptic cylinder positioned over a flat plate. Although there have been a number of experimental investigations on such flows, numerical investigations is limited due to its complexity in grid generation. Also wake induced from the elliptic cylinder got less attention in this regard. A numerical study of this type of flow for laminar Reynolds number 500 is considered here. Figure 3 shows the scheme of computational domain of the present research work.

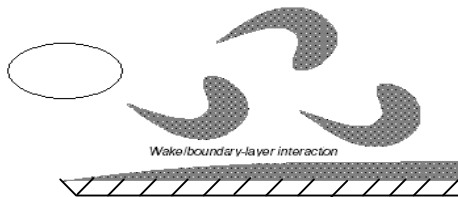


Figure 1. Interaction in a simplified geometry

MATHEMATICAL MODELING

Figure 2 shows the geometry of the elliptic cylinder having major and minor axis of lengths $2a$ and $2b$ respectively and axis ratio ($AR = b/a$) of 0.6, in an otherwise uniform flow, U can be modeled by unsteady 2-D Navier-Stokes equation neglecting body forces,

$$\rho \frac{\partial V}{\partial t} + \rho (V \cdot \nabla) V = -\nabla P + \mu \nabla^2 V \tag{1}$$

Dimensionless analysis

The dimensionless quantities are,

$$V' = \frac{V}{U}, \quad x' = \frac{x}{c}, \quad y' = \frac{y}{c}, \quad P' = \frac{P}{\rho U^2},$$

$$t' = \frac{Ut}{c} \quad \text{also,} \quad \nabla = \frac{1}{c} \nabla' \quad \text{and}$$

$$\nabla^2 = \frac{1}{c^2} \nabla'^2$$

where, c stands for the focal distance of the ellipse defined by, $c = \sqrt{a^2 - b^2}$.

Now equation (1) in dimensionless form,

$$\rho \frac{\partial V' U}{\partial \left(\frac{t' c}{U}\right)} + \rho \left(V' U \cdot \frac{1}{c} \nabla'\right) V' U = -\frac{1}{c} \nabla' P' \rho U^2 + \mu \frac{1}{c^2} \nabla'^2 V' U$$

$$\text{or, } \frac{\partial V'}{\partial t'} + (V' \cdot \nabla') V' = -\nabla' P' + \frac{2}{Re_{2c}} \nabla'^2 V' \tag{2}$$

$$\text{Where } Re_{2c} = \frac{\rho U (2c)}{\mu}$$

Equation (2) is the dimensionless form of 2-D unsteady Navier-Stokes equation.

Dimensionless form of conservation of mass,

$$\nabla' \cdot V' = 0 \tag{3}$$

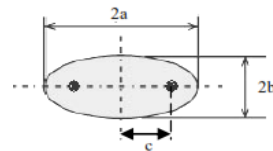


Figure 2. Geometry of the elliptic cylinder

Equation (3) along with the compressibility constraint, equation (2) is used for the present numerical computation.

In the present computation dimensionless time is considered as $\tau = \frac{Ut}{c}$ which was used by Badr, Dennis and Kocabiyik (2001) where they used the vorticity/stream function formulation of unsteady 2-D Navier-Stokes equation.

Boundary conditions

The computational Domain is subjected to the following initial and boundary conditions,

$$\text{Initial condition: } (u, v) \Big|_{t=0} = (U, V)$$

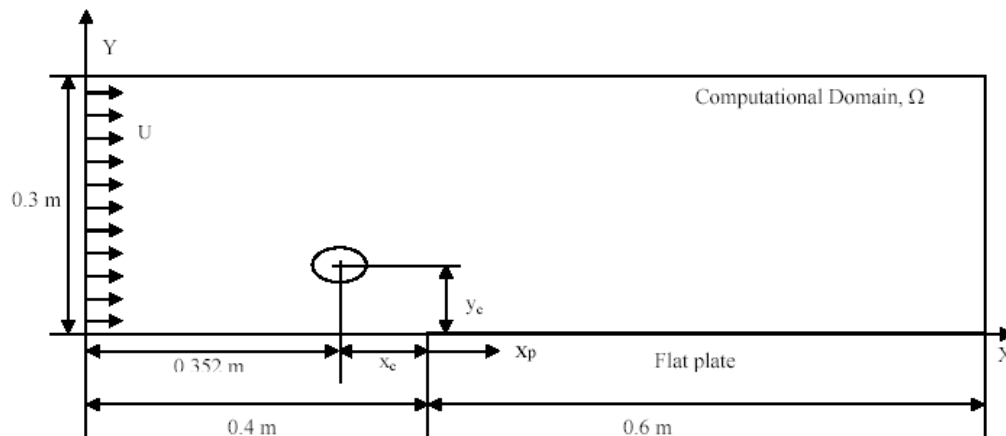


Figure 3. Scheme of the computational domain (not to scale)

The boundary conditions:

- An inflow boundary condition is applied at the left boundary: $\mathbf{V} = \mathbf{U}$ i.e. $u = U$ and $v = 0$
- Slip boundary condition is applied at the lower left boundary: $\frac{\partial u}{\partial y} = 0$, $v = 0$
- No-slip velocity condition for all velocity components on all solid walls. So,
 - On the plate surface, $\mathbf{V} = 0$ i.e. $u = v = 0$.
 - On the surface of the cylinder, also $\mathbf{V} = 0$ i.e. $u = v = 0$.
- An open boundary condition is applied at the upper boundary of the domain.

$$(-p\mathbf{I} + \mu(\nabla \mathbf{V} + (\nabla \mathbf{V})^T)) \mathbf{n} = 0$$

- An outflow boundary condition is applied at the right boundary: $\mu(\nabla \mathbf{V} + (\nabla \mathbf{V})^T) \mathbf{n} = 0$ and $p = p_0$

RESULTS AND DISCUSSION

The first section of the result is concerned with the “code validation” i.e. the results obtained from the elliptic cylinder in uniform flow is compared with the results of the published data available in literature. The second section deals with the results of the present numerical simulation of the two dimensional boundary layer development on the surface of a flat plate under the influence of passing wake vortices induced from an elliptic cylinder and the effects of the relative position of the cylinder to the plate at $Re_{2c} = 500$. The relative position between the center of the cylinder and the plate leading edge considered here are $x_c/2c = -3$, $y_c/2c = 1$; $x_c/2c = 0$, $y_c/2c = 1$; $x_c/2c = 3$, $y_c/2c = 1$ and $x_c/2c = 0$, $y_c/2c = 0.75$. The method of the solution and the accuracy of the numerical scheme of elliptic cylinder in uniform

flow is verified here for Reynolds number $Re_{2c} = 1000$, the angle of attack of $\alpha = 0^\circ$ and cylinder minor-major axis ratio $AR = 0.6$. In order to verify the present numerical scheme used in this work, the initial flow for the problem of flow field of the elliptic cylinder only is considered. The Figures 4 and 5 presenting the instantaneous streamline and drag and lift coefficients found in the present problem show a good agreement with the numerical solution of Badr, Dennis and Kocabiyik (2001).

Figure 4 shows that at the start of motion, the wake cavity behind the cylinder contains a symmetrical pair of equal and opposite recirculating-flow regions (upper clockwise and lower counter-clockwise vortex pairs) on either side of the wake whose length grows (due to viscous stresses) with the increase of time τ . The drag coefficient, C_D can be split into two parts, $C_D = C_{DF} + C_{DP}$, where, C_{DF} and C_{DP} are the friction and pressure components of the drag coefficient. The calculated values of the drag coefficients for $Re_{2c} = 1000$ and $\alpha = 0^\circ$, when the flow is symmetric about the major axis are plotted in Fig. 5. The figure shows that the contribution of frictional force to the total drag coefficient C_D is relatively small.

Instantaneous Stream Lines

Figure 6 shows the stream lines development of the flow field for $\tau = 350$ of the present numerical problem. The flow fields are found to be in the laminar vortex shedding regime. As the wake moves downstream, it starts interaction with the boundary layer on the plate by advecting low speed fluid from the wall into the outer region and high speed fluid from the core towards the wall, as rollers of

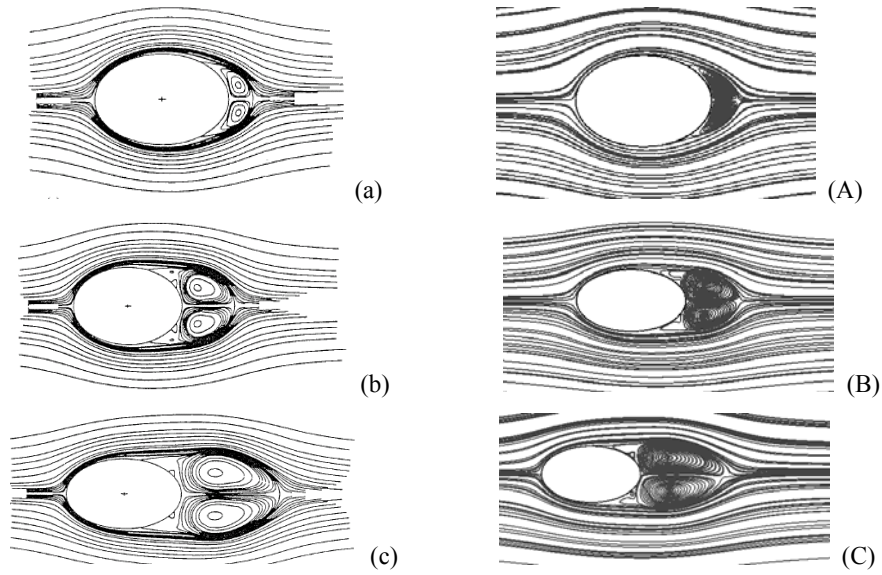


Figure 4. Comparison of Instantaneous streamlines of the flow for $Re_{2c}=1000$, and $\alpha = 0^0$: (a,A) $\tau = 2.0$; (b,B) $\tau = 5.0$; (c,C) $\tau = 10.0$. (a-c) Flow visualization by Badr, Danis and Kocabiyik and (A-C) Present Finite Element Computation.

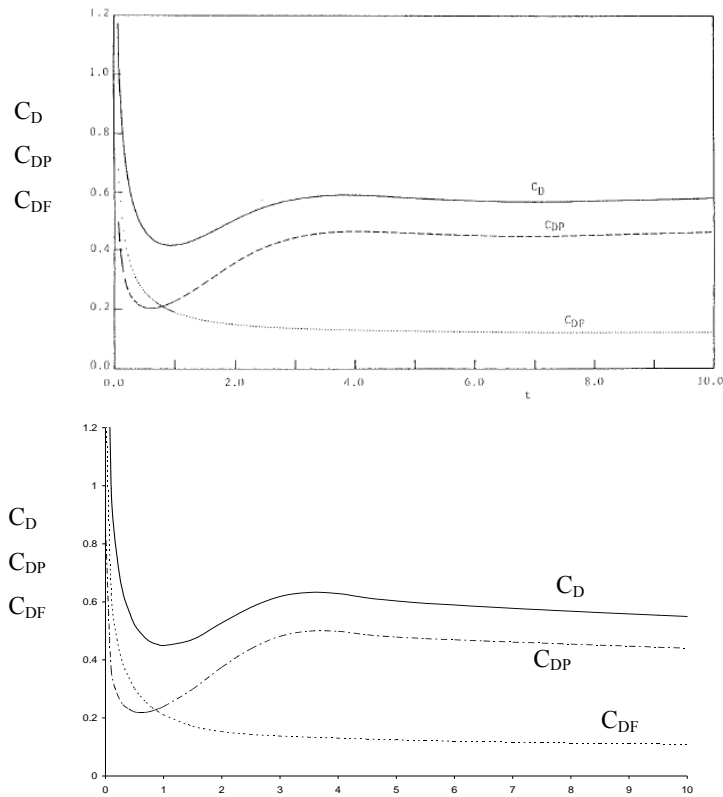


Figure 5. Variation of the Drag Coefficients C_D , C_{DF} , and C_{DP} with τ at $Re_{2c} = 1000$ and $\alpha = 0^0$. (a) results from Badr, Danis and Kocabiyik, (b) Present Finite Element Computation.

alternating rotation are convected above the boundary layer and so the shape of the streamlines found in the figures are in wavy shape. The wake spreads outward from the source until its energy is lost, usually by friction or dispersion and becomes weaker. Strong inviscid-viscid interaction takes place in the form of an eruption in the boundary layer and eruptions and the vortices penetrate into the wake region and weaken the vortex formation in the shear layer.

An interesting feature also found for cylinder to plate relative position $x_c/2c = 0$, $y_c/2c = 0.75$, is that when the wake interacts with the plate boundary layer, some vortices or bubbles develops there. It can be explained in the way that the molecular diffusion

in some places in the laminar boundary layer is often small as compared with the existing pressure gradients of the plate. The transport of streamwise momentum across the boundary layer is therefore not sufficiently large to prevent a deceleration of the innermost fluid which eventually begins the flow separation. The separated shear layer which is formed curves back to the plate surface and forms a shallow region of reverse flow called separation bubble.

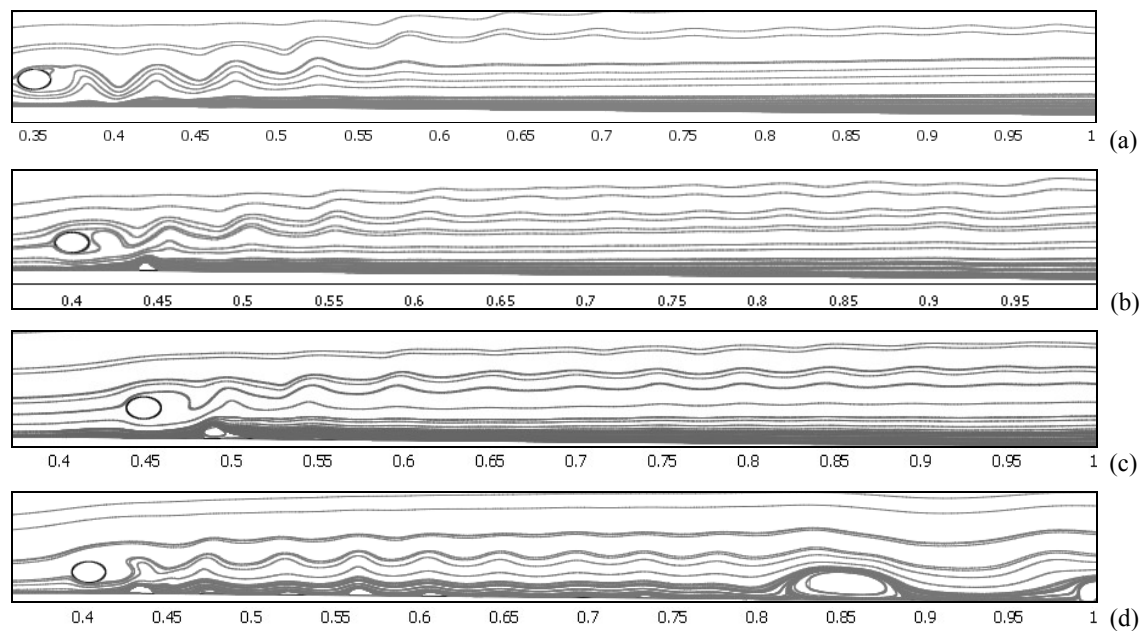


Figure 6. Instantaneous streamlines on the flow field for $Re_{2c}=500$, $\tau = 500$, (a) $x_c/2c = -3$, $y_c/2c = 1$ (b) $x_c/2c = 0$, $y_c/2c = 1$, (c) $x_c/2c = 3$, $y_c/2c = 1$ and (d) $x_c/2c = 0$, $y_c/2c = 0.75$.

Instantaneous velocity profile

An overall picture of the boundary layer-cylinder wake interaction could be obtained, by studying the velocity profiles (Fig. 7). From the visualization of the velocity profiles, it can be said that the shape of the profiles are largely dependent on the combined effect of Reynolds number, cylinder to plate relative position, size of the wake, the presence and size of the separation bubble. But in general, in every velocity profile, two regions could be identified. The first one is a wake region which appears downstream of the cylinder, creating a velocity defect which gradually disappears with the streamwise distance. The second is the boundary layer region. In this case the velocity distribution, up to the point of interaction, followed the shape of Blasius profile, indicating that the

boundary layer is still laminar. Moving forward from the plate leading edge to the downstream, it is found that the shape of the streamlines are wavy and the velocity profile is not as Blasius because of the effect of the shed vortices to the near wall region. In this region the wake from the cylinder perturbs the boundary layer by advecting low-speed fluid from the wall into outer region and, and high speed fluid from the core towards the wall, as rollers of alternating rotation are convected above the boundary layer. Thus approximately S-shaped velocity profile under the influence of wake vortices is identified. As the wake decays, the advection effect becomes less significant.

Figure 8 presents the undisturbed flow field on the flat plate. Comparing to Fig. 7 it is found that the shapes of the velocity profile for all axial

locations of undisturbed flow are similar to Blasius profile. It also shows that the thickness of the velocity profile increases with the increase of

axial distance from the leading edge of the plate.

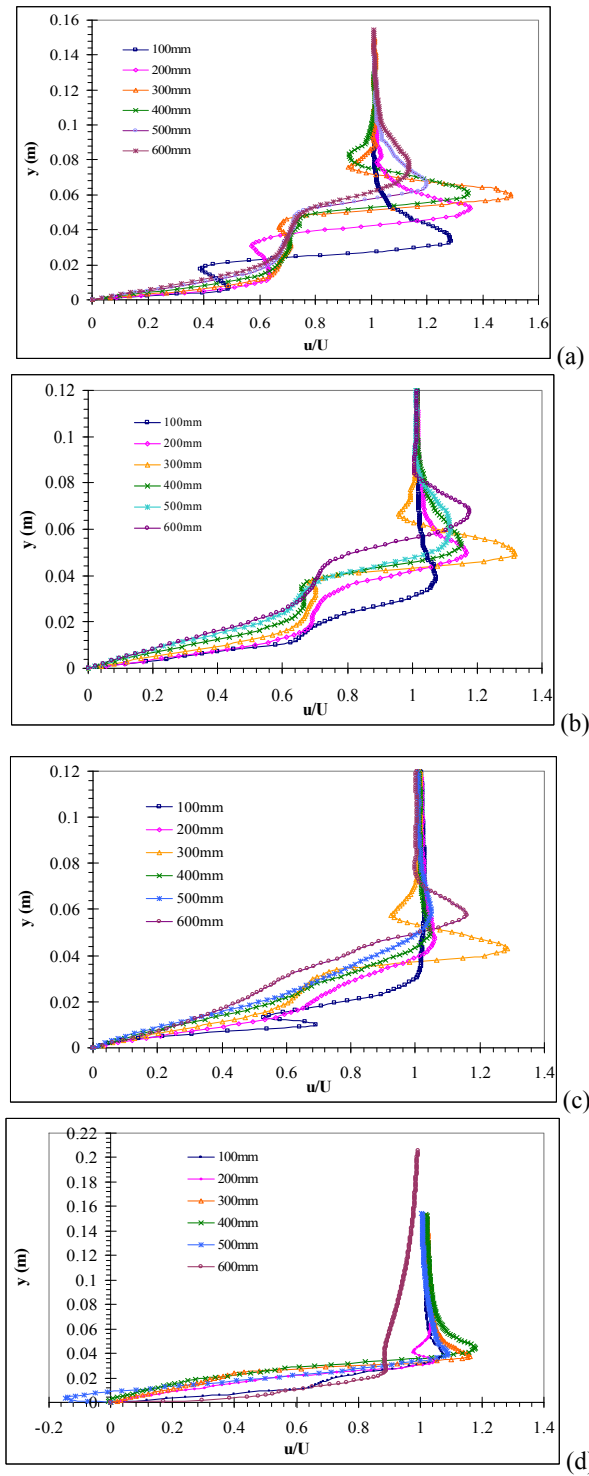


Figure 7. Instantaneous velocity distribution on different flat plate axial locations for $\tau = 500$, $Re_{2c}=500$, (a) $x_c/2c = -3$, $y_c/2c = 1$ (b) $x_c/2c = 0$, $y_c/2c = 1$, (c) $x_c/2c = 3$, $y_c/2c = 1$ and (d) $x_c/2c = 0$, $y_c/2c = 0.75$.

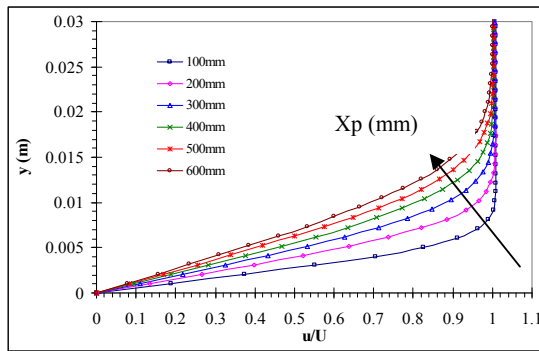


Figure 8. Undisturbed profile of velocity distribution on different flat plate axial location, for $Re = 500$.

In case of disturbed flow, for a particular gap ratio (cylinder to plate relative position), it is clearly observed that the boundary layer thickness increases with the increase of plate axial location. This is due to, wake vortices widen further downstream and thus the merging of wake vortices with boundary layer occurs in large scale. More wake vorticity elements available in the boundary layer which can interact more with increasing plate axial locations. Thus velocity deficit starts (for wake region) somewhat earlier in upward direction from the plate with increasing the streamwise positions. The velocity profile at $x_p = 500$ mm of case (d) exhibit a negative behavior i.e. $u/U < 0$ indicating the presence of separation bubble on the plate surface.

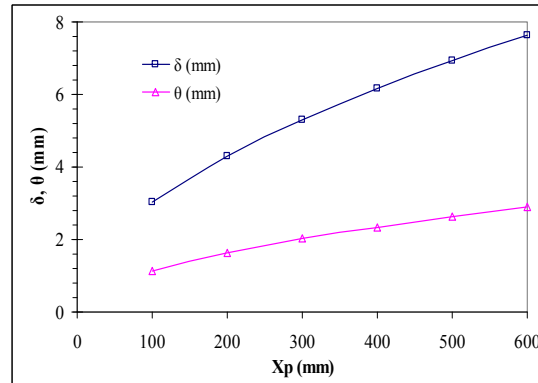
Boundary layer integral parameter

Figure 9 shows the variation of displacement thickness, momentum thickness and shape factor with the plate axial location for undisturbed flow condition. According to these figures, both the displacement thickness and momentum thickness increases with the increase in plate axial length (for laminar flat plate both δ and θ are proportion to $X_p^{1/2}$) but ultimately their ratio called the shape factor remain same i.e. $H \approx 2.6$ indicating that the flow is laminar.

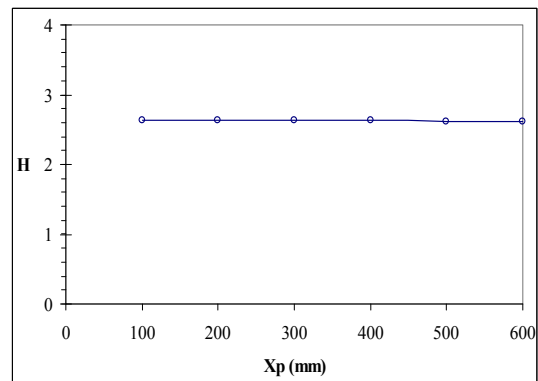
The boundary layer integral parameter, shape factor (H), is of particular interest to turbine designer, since it provides an accurate first estimation of the quality of the designed blade. Figure 10 shows that the boundary layer integral parameters exhibit the fluctuating behavior comparing to undisturbed boundary layer analysis where $H \approx 2.6$ indicating that the flow is laminar.

For a particular cylinder to plate relative position, the trend of shape factor exhibit that with the increase of plate axial distance, the amplitude of the fluctuations gradually decreases. This may be due the fact that there is strong interaction near the plate leading edge

where the size of the wake is small (sharp sinusoidal behavior of streamlines showing peak and valleys) and as the wake passes downstream of the plate the interaction is weaker and the wake size becomes larger (sinusoidal behavior of streamlines almost damped out).



(a)



(b)

Figure 9. Spatial variation of (a) \square -displacement thickness (δ), Δ -momentum thickness (θ) and (b) \circ -shape factor (H) of undisturbed flow over the flat plate for $Re_{2c} = 500$.

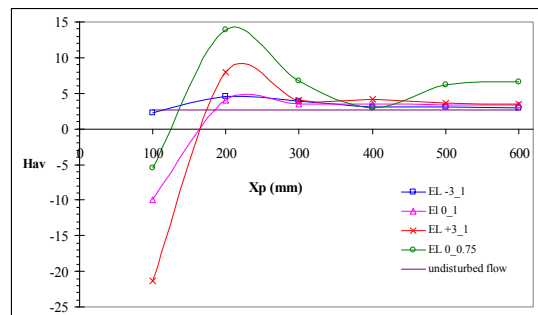


Figure 10. Average shape factor (H_{av}) variation with plate stream-wise locations at different cylinder to plate relative position. for $Re_{2c} = 500$.

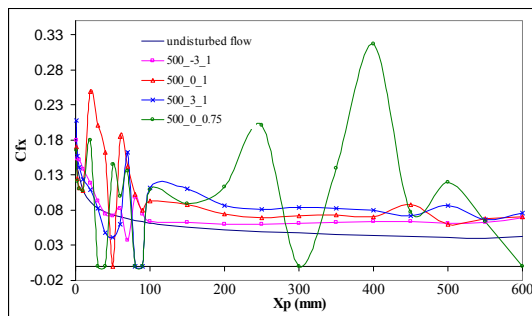


Figure 11. Variation of skin friction with different plate axial location for $\tau = 500$, $Re_{2c} = 500$ at different elliptic cylinder to plate relative position.

Skin friction

Figure 11 shows the variation of skin friction with the plate streamwise axial position. For the undisturbed flow case and also for the disturbed cases with the presence of cylinder wake, it is found that as the axial distance of the plate increases, the skin friction decreases.

From the figure it is clear that, as the cylinder moves closer to the plate, the interaction between the cylinder wake and plate boundary layer becomes stronger and the skin friction increases. The value of skin friction for undisturbed flow on the flat plate found lower (not very large amount) than that of the disturbed flow. In each case, the skin friction starts from a perturbed laminar value that does not coincide with the Blasius profile.

CONCLUSION

Two types of boundary layer-wake interaction are obtained from the computations, one is the strong wake-boundary layer interaction and another is the weak wake-boundary layer interaction. The intensity of interaction greatly depends on plate streamwise location and the gap ratio between the plate and the cylinder. The lower the gap ratio, the more rapidly the wake loses its coherence, and the more unstable the boundary layer is to perturbation. The impingement of wake on the boundary layer causes velocity and momentum deficit on the flow field. Shape factor is also disturbed by wake vortices. The wake vortices and separation bubbles changes the thicknesses randomly and consequently the shape factor also.

Wake vorticity elements can always generate from the cylinder and affects on the transition in boundary layers. Transitional phenomena are crucially important to the design of the compressor and the turbines. In the former, about half the loss of stage efficiency at the design point owes to skin friction, which is several times larger in a turbulent

boundary layer than in its laminar counterpart. The separation bubble, which usually is laminar at the point of separation, if transition occurs, will likely reattach to the blade surface and the loss in efficiency is limited. Under some circumstances, the transitional process is slow and the flow reattachment point may move far downstream on the suction surface and the large separated region cause severe losses in stage efficiency.

REFERENCES

- [1] Victor O., Ugo Piomelli, and Meelan M. Choudhari, (2006), "Numerical simulations of boundary layer transition induced by a cylinder wake", *J. Fluid Mech.*, vol. 547, pp. 413–441.
- [2] Badr H.M., Dennis S.C.R. and Kocabiyik S., (2001), "Numerical simulation of the unsteady flow over an elliptic cylinder at different orientations", *International Journal for Numerical Methods in Fluids*; 37: 905-931.
- [3] Choi, J.-H. and Lee, S.-J., (2000), "Ground effect of flow around an elliptic cylinder in a turbulent boundary layer", *Journal of Fluids and Structures*, vol. 14, pp. 697-709.
- [4] Kyriakides, N. K., Kastrinakis, E.G., Nychas, S.G., Goulas, A., (1996), "Boundary layer transition induced by a von karman vortex street wake", *IMEchE, PartG: Journal of Aerospace Engineering*, vol. 210, pp. 167-179.
- [5] Liu, X., and Rodi, W., (1991), "Experiments on transitional boundary layers with wake induced unsteadiness", *J. Fluid Mech.*, vol. 231, pp. 229-256.
- [6] Taneda S., (1977), 'Visual study of unsteady separated flows around bodies', *Progress in Aerospace Science*, vol. 17, pp. 287–348.
- [7] Taneda S., (1972), 'The development of the lift of an impulsively started elliptic cylinder at incidence', *Journal of the Physics Society of Japan*, vol. 33, pp. 1706–1711.